Supplement of Atmos. Chem. Phys., 22, 7619–7630, 2022
https://doi.org/10.5194/acp-22-7619-2022-supplement

Atmospheric Chemistry and Physics
Open Access
EGU

Supplement of

The chemical composition and mixing state of BC-containing particles and the implications on light absorption enhancement

Jiaxing Sun et al.

Correspondence to: Yele Sun (sunyele@mail.iap.ac.cn)

1.1 Positive matrix factorization (PMF) analysis

PMF analysis was used to identify the effect of different mixing states on light absorption enhancement (E_{abs}). The input of the PMF analysis included $b_{abs,\ total}$, $b_{abs,\ BCpure}$ and 11 major types of BC-containing particles ($b_{abs,\ total}$ was obtained from the linear interpolation of measured ambient absorptions adjacent to the thermodenuder (TD) line and $b_{abs,\ BCpure}$ was defined as the thermodenuded particle absorption in the TD line at $T > 200$°C), and the uncertainties were determined by the following algorithms (Polissar et al., 1998; Petit et al., 2014) (Eq. 1):

$$U_{ij} = \begin{cases} \frac{5}{6} * LOD_i & \text{if } C_j \le LOD_i \\ \sqrt{u_i^2 C_i^2 + LOD_i^2} & \text{if } C_j \ge LOD_i \end{cases} \quad (1)$$

LOD_i represents the limit of detection and u_i represents the relative uncertainty (in %) for each variable. The final uncertainty (U_{ij}) is determined by the LOD and u, which represents the ith species in the jth row. The LODs for the species were calculated as 3 times the standard deviation calculated during the clean period. After a careful evaluation of the PMF solutions, five factors (Factor1, Factor2, Factor3, Factor4 and Factor5) in Beijing and four factors (FactorA, FactorB, FactorC and FactorD) in Gucheng were chosen to study the influence of different mixing states on E_{abs}.

1.2 Method of estimating the direct radiative forcing

Based on E_{abs} for each factor and the contribution of that factor to $b_{abs,\ BCpure}$, we further simply estimated the direct radiative forcing (ΔF_R) caused by BC-containing particles with their mixing state at the top-of-atmosphere (TOA), suggested by a previous study (Chylek and Wong, 1995; Chen and Bond, 2010). The modified version of the equation is given as below:

$$\Delta F_{R,fi} = \int -\frac{1dS(\lambda)}{4d\lambda} \tau_{atm}^2(\lambda)(1 - F_c)[(1 - a_s)^2 2\beta\tau_{scat,fi}(\lambda) - 4a_s\tau_{abs,fi}(\lambda)]d\lambda \quad (2)$$

where S is the solar irradiance (W m^{-2}), τ_{atm} is the atmospheric transmission (unitless), F_c is the fractional cloud amount (0.6 unitless), a_s is the surface reflectance (0.19 unitless), β is the backscatter fraction (0.29 unitless) (Charlson et al., 1992; Bond and Bergstrom, 2006; Wang et al., 2019), and τ_{scat} and τ_{abs} are the aerosol scattering and absorption optical depths (unitless), respectively. The wavelength-dependent S(λ) and $\tau_{atm}(\lambda)$ are derived from the ASTM G173-03 reference spectra (Chen and Bond, 2010). τ_{scat} and τ_{abs} can be estimated as $\tau_{scat}(\lambda) = b_{sca}(\lambda) \times$ Heff and $\tau_{abs}(\lambda) = b_{abs}(\lambda)\ E_{abs} \times$ Heff, respectively, where Heff is the effective height (Wang et al., 2019) derived from the relationship between the aerosol optical depth τ (= τ_{scat} + τ_{abs}, available from the Aerosol Robotic Network data archive) and the light extinction coefficient b_{ext} (= b_{abs} + b_{sca}, derived from a photoacoustic extinctiometer (PAX)), shown in Table S2. And ΔF_R is the sum of all factor values of $\Delta F_{R,\ fi.}$

Table S1. Summary of abbreviations and descriptions of BC-containing particle types.

Description of type or species	Typical ions	Abbreviation	References
BC only from biomass burning	$39K^+$ (peak area >1500) and two of the signals in 45$[CHO_2]^-$, 59$[C_2H_3O_2]^-$ and 73$[C_3H_5O_2]^-$ (peak area >200).	BB_{pure}	(Silva et al., 1999; Healy et al., 2010)
BC only from coal combustion	$7Li^+$ (peak area >200) or 23$[Na]^+$, 27$[Al]^+$, 43$[AlO]^-$ (peak area >200) or 80$[SO_3]^-$, 97$[HSO_4]^-$ (relative peak area >2%).	CC_{pure}	(Zhang et al., 2009; Healy et al., 2010)
BC only from traffic emission	55$[Mn]^+$ (peak area >200 without Na^+ and Al^+) or 40$[Ca]^+$ (with abundant nitrate) or 79$[PO3]^-$ (with abundant nitrate) or 51$[V]^+$ and 67$[VO]^+$ (peak area >200).	TR_{pure}	(Yang et al., 2017)
BC internally mixed more than one sources	Same as the above.	MixSource	
BC internally mixed with nitrate	46$[NO_2]^-$ and 62$[NO_3]^-$ (relative peak area >70%).	BC_N	The selected conditions about nitrate, sulfate and OC (Dall'Osto and Harrison, 2012; Sierau et al., 2014; Chen et al., 2016; Zhou et al., 2016; Arndt et al., 2017; Cheng et al., 2017; Zhang et al., 2019).
BC internally mixed with sulfate	97$[HSO_4]^-$ (relative peak area >70%).	BC_S	
BC internally mixed with nitrate and sulfate	46$[NO_2]^-$ and 62$[NO_3]^-$ are comparable with 97$[HSO_4]^-$.	BC_{NS}	
BC internally mixed with OC and nitrate	three of the signals in 37$[C_3H]^+$, 43$[C_2H_3O]^+$, 51$[C_4H_3]^+$ and 63$[C_5H_3]^+$ (relative peak area >2%) with nitrate.	$BCOC_N$	
BC internally mixed with OC and sulfate	three of the signals in 37$[C_3H]^+$, 43$[C_2H_3O]^+$, 51$[C_4H_3]^+$ and 63$[C_5H_3]^+$ (relative peak area >2%) with sulfate.	$BCOC_S$	
BC internally mixed with OC, nitrate, and sulfate	three of the signals in 37$[C_3H]^+$, 43$[C_2H_3O]^+$, 51$[C_4H_3]^+$ and 63$[C_5H_3]^+$ (relative peak area >2%) with comparable nitrate and sulfate.	$BCOC_{NS}$	

Table S2. Summary of the relationship between the aerosol optical depth and the light extinction coefficient measured by PAX at both sites. The slope represents the effective height and *r* represents the correlation coefficient.

	Beijing	Gucheng
Effective Height (m)	711	554
r	0.73	0.51

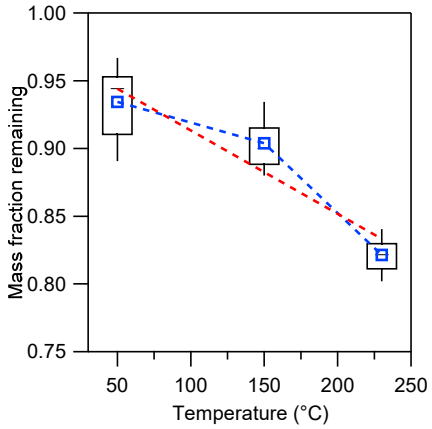

Figure S1. Loss of pure BC particles in the thermodenuder under different temperatures.

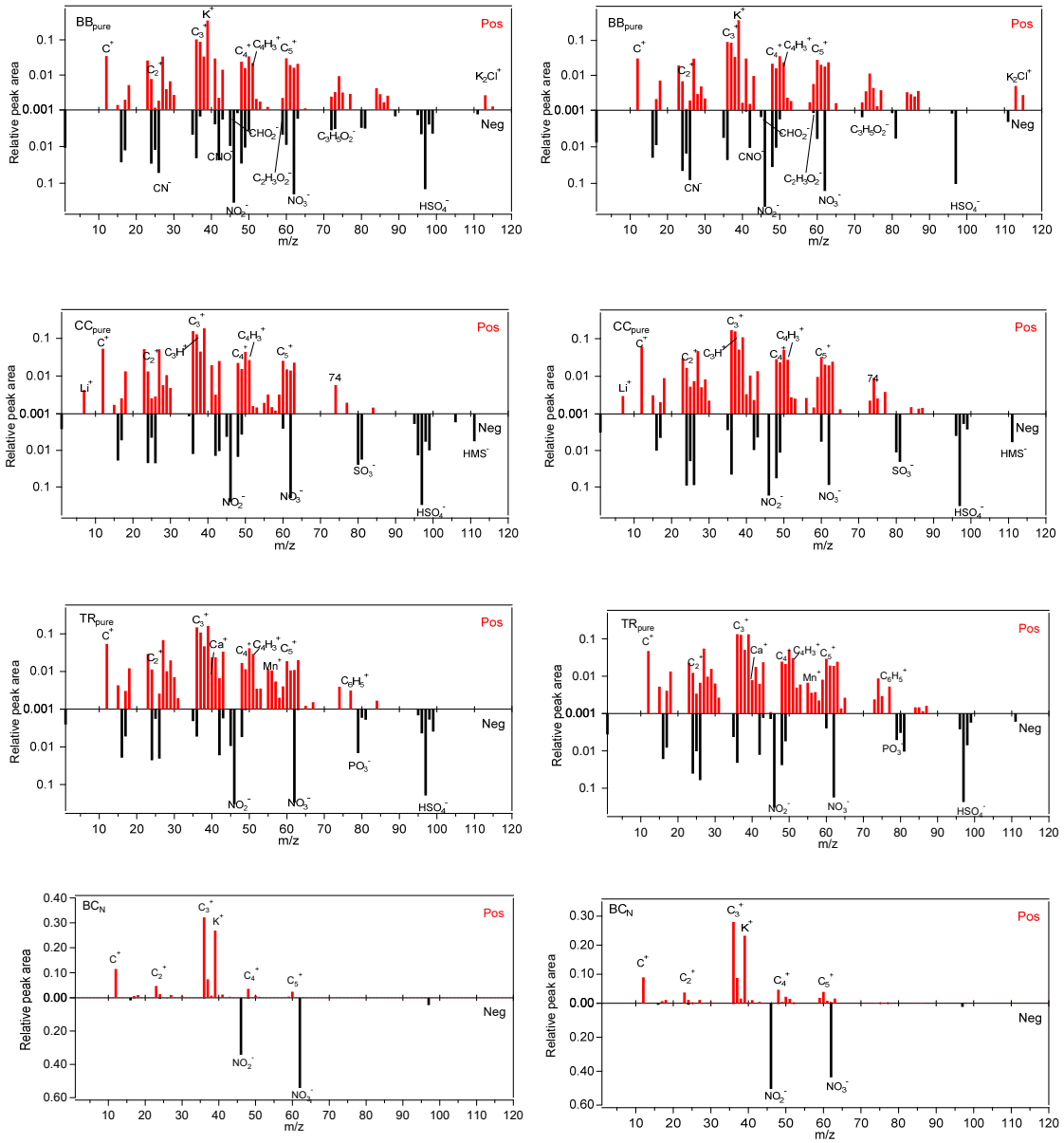

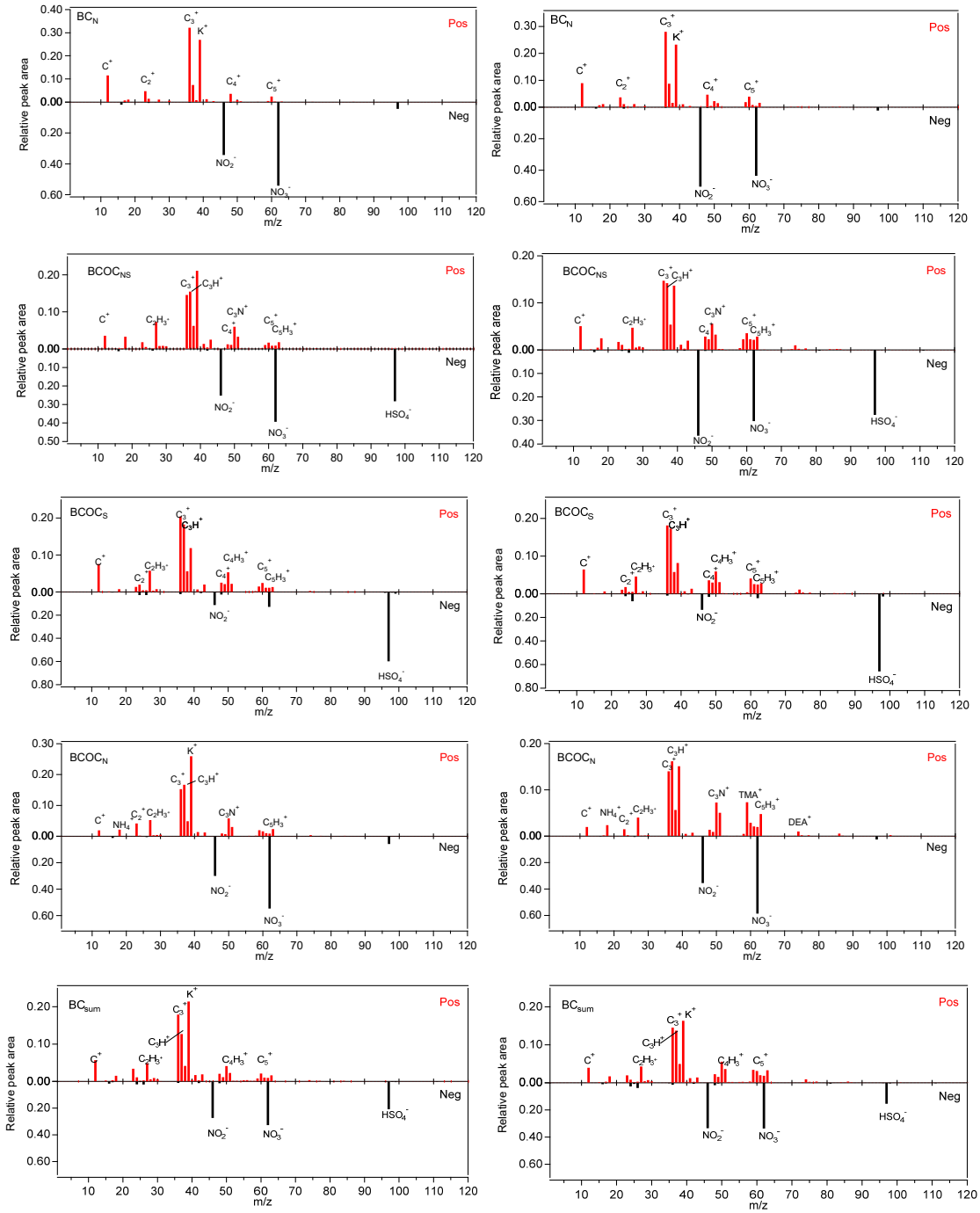

Figure S2. Average mass spectra of six types of BC-containing particles and total BC-containing particles in Beijing (left panel) and Gucheng (right panel).

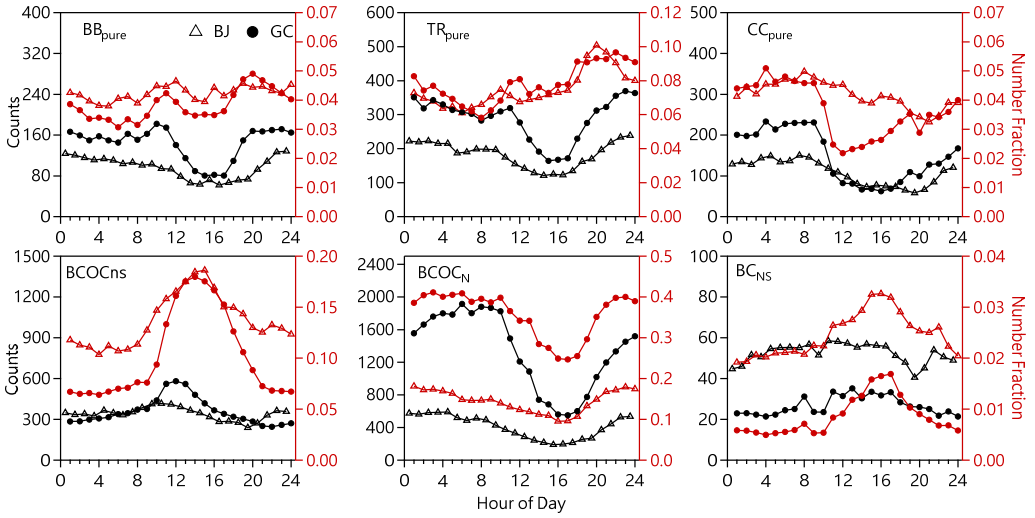

Figure S3. Diurnal variations of six types of BC-containing particles in Beijing (BJ)and Gucheng (GC).

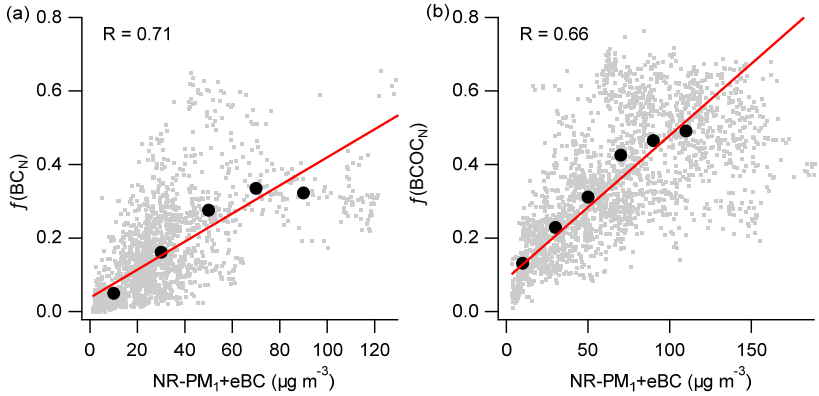

Figure S4. Relationship between the sum of the mass concentration of NR-PM$_1$ and eBC with (a) number fraction of BC$_N$ in BJ and (b) number fraction of BCOC$_N$ in GC (for the definitions of NR-PM$_1$ and eBC, see the main text).

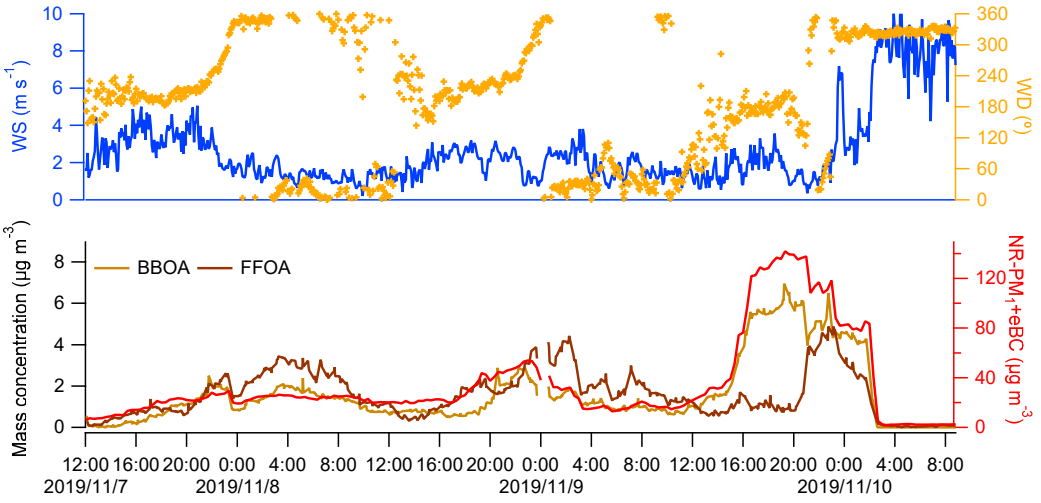

Figure S5. Time series of wind speed (WS), wind direction (WD), NR-PM$_1$+eBC, FFOA and BBOA in Case2 (with FFOA standing for fossil fuel-related organic aerosol (OA) and BBOA for biomass burning OA).

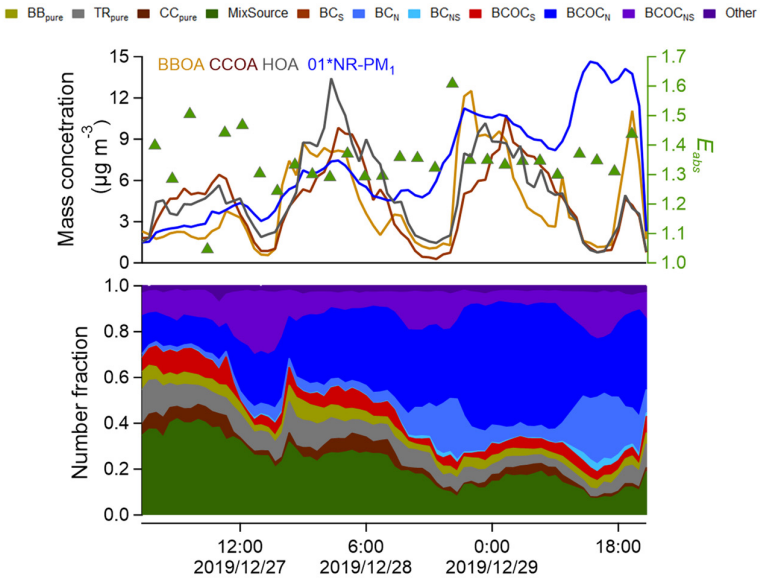

Figure S6. Temporal variations of E_{abs}, number fractions of BC-containing particle types and mass concentration of species during pollution case in GC.

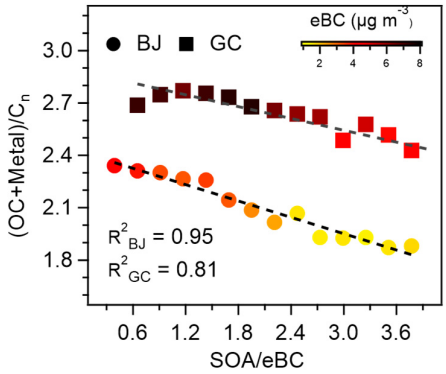

Figure S7. Relationships between peak area ratio of (OC + Metal)/C_n and mass concentration ratio of SOA/eBC (SOA = LO-OOA + MO-OOA in BJ and = OOA + aq-OOA in GC); for the definitions of OC, SOA, eBC, LO-OOA, MO-OOA, OOA and aq-OOA, see the main text.

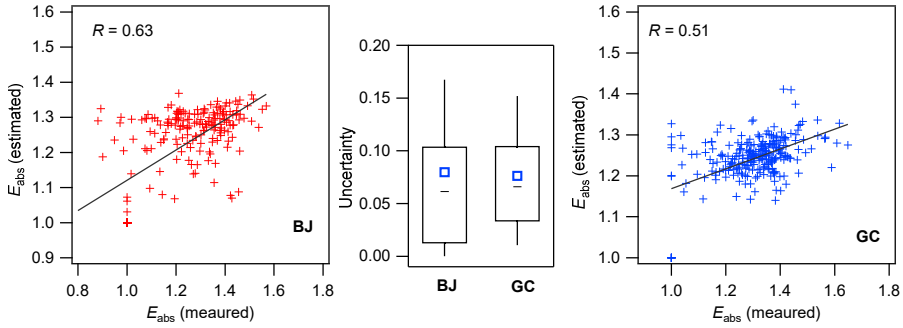

Figure S8. Comparison between measured and estimated E_{abs} in BJ and GC. The uncertainty is determined by the absolute ratio of ($E_{abs,\ measured}$ - $E_{abs,\ estimated}$) to $E_{abs,\ measured}$.

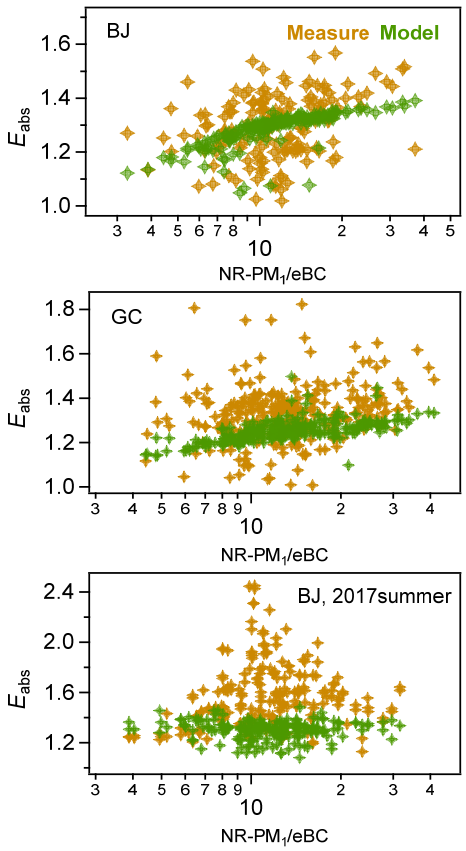

Figure S9. Comparison between measured data and model results.

References

Arndt, J., Sciare, J., Mallet, M., Roberts, G. C., Marchand, N., Sartelet, K., Sellegri, K., Dulac, F., Healy, R. M., and Wenger, J. C.: Sources and mixing state of summertime background aerosol in the north-western Mediterranean basin, Atmos. Chem. Phys., 17, 6975-7001, 10.5194/acp-17-6975-2017, 2017.

Bond, T. C. and Bergstrom, R. W.: Light absorption by carbonaceous particles: an investigative review, Aerosol Sci. Technol., 40, 27-67, 10.1080/02786820500421521, 2006.

Charlson, R. J., Schwartz, S. E., Hales, J. M., Cess, R. D., Coakley, J. A., Hansen, J. E., and Hofmann, D. J.: Climate forcing by anthropogenic aerosols, Science, 255, 423-430, 1992.

Chen, Y. and Bond, T. C.: Light absorption by organic carbon from wood combustion, Atmos. Chem. Phys., 10, 1773-1787, 2010.

Chen, Y., Cao, J., Huang, R., Yang, F., Wang, Q., and Wang, Y.: Characterization, mixing state, and evolution of urban single particles in Xi'an (China) during wintertime haze days, Sci. Total Environ., 573, 937-945, 10.1016/j.scitotenv.2016.08.151, 2016.

Cheng, C., Li, M., Chan, C. K., Tong, H., Chen, C., Chen, D., Wu, D., Li, L., Wu, C., Cheng, P., Gao, W., Huang, Z., Li, X., Zhang, Z., Fu, Z., Bi, Y., and Zhou, Z.: Mixing state of oxalic acid containing particles in the rural area of Pearl River Delta, China: implications for the formation mechanism of oxalic acid, Atmos. Chem. Phys., 17, 9519-9533, 10.5194/acp-17-9519-2017, 2017.

Chylek, P. and Wong, J.: Effect of aerosols on global budget, Geophys. Res. Lett., 22, 929-931, 1995.

Dall'Osto, M. and Harrison, R. M.: Urban organic aerosols measured by single particle mass spectrometry in the megacity of London, Atmos. Chem. Phys., 12, 4127-4142, 10.5194/acp-12-4127-2012, 2012.

Healy, R. M., Hellebust, S., Kourtchev, I., Allanic, A., O'Connor, I. P., Bell, J. M., Healy, D. A., Sodeau, J. R., and Wenger, J. C.: Source apportionment of PM2.5 in Cork Harbour, Ireland using a combination of single particle mass spectrometry and quantitative semi-continuous measurements, Atmos. Chem. Phys., 10, 9593-9613, 10.5194/acp-10-9593-2010, 2010.

Petit, J. E., Favez, O., Sciare, J., Canonaco, F., Croteau, P., Močnik, G., Jayne, J., Worsnop, D., and Leoz-Garziandia, E.: Submicron aerosol source apportionment of wintertime pollution in Paris, France by double positive matrix factorization (PMF2) using an aerosol chemical speciation monitor (ACSM) and a multi-wavelength Aethalometer, Atmos. Chem. Phys., 14, 13773-13787, 10.5194/acp-14-13773-2014, 2014.

Polissar, A. V., Hopke, P. K., Paatero, P., Malm, W. C., and Sisler, J. F.: Atmospheric aerosol over Alaska: 2. Elemental composition and sources, J. Geophys. Res.-Atmos., 103, 19045-19057, 10.1029/98JD01212, 1998.

Sierau, B., Chang, R. Y. W., Leck, C., Paatero, J., and Lohmann, U.: Single-particle characterization of the high-Arctic summertime aerosol, Atmos. Chem. Phys., 14, 7409-7430, 10.5194/acp-14-7409-2014, 2014.

Silva, P. J., Liu, D. Y., Noble, C. A., and Prather, K. A.: Size and chemical characterization of individual particles resulting from biomass burning of local Southern California species, Environ. Sci. Technol., 33, 3068-3076, 10.1021/es980544p, 1999.

Wang, Q., Ye, J., Wang, Y., Zhang, T., Ran, W., Wu, Y., Tian, J., Li, L., Zhou, Y., Hang Ho, S. S., Dang, B., Zhang, Q., Zhang, R., Chen, Y., Zhu, C., and Cao, J.: Wintertime optical properties of primary and secondary brown carbon at a regional site in the North China Plain, Environ. Sci. Technol., 53, 12389-12397, 10.1021/acs.est.9b03406, 2019.

Yang, J., Ma, S., Gao, B., Li, X., Zhang, Y., Cai, J., Li, M., Yao, L., Huang, B., and Zheng, M.: Single particle mass spectral signatures from vehicle exhaust particles and the source apportionment of on-line PM2.5 by single particle aerosol mass spectrometry, Sci. Total Environ., 593, 310-318, 10.1016/j.scitotenv.2017.03.099, 2017.

Zhang, J., Huang, X., Chen, Y., Luo, B., Luo, J., Zhang, W., Rao, Z., and Yang, F.: Characterization of lead-containing atmospheric particles in a typical basin city of China: Seasonal variations, potential source areas, and responses to fireworks, Sci. Total Environ., 661, 354-363, 10.1016/j.scitotenv.2019.01.079, 2019.

Zhang, Y., Wang, X., Chen, H., Yang, X., Chen, J., and Allen, J. O.: Source apportionment of lead-containing aerosol particles in Shanghai using single particle mass spectrometry, Chemosphere, 74, 501-507, 10.1016/j.chemosphere.2008.10.004, 2009.

Zhou, Y., Huang, X. H. H., Griffith, S. M., Li, M., Li, L., Zhou, Z., Wu, C., Meng, J., Chan, C. K., Louie, P. K. K., and Yu, J. Z.: A field measurement based scaling approach for quantification of major ions, organic carbon, and elemental carbon using a single particle aerosol mass spectrometer, Atmos. Environ., 143, 300-312, 10.1016/j.atmosenv.2016.08.054, 2016.